

A Joint Learning Framework for Bridging Defect Prediction and Interpretation

Guifang Xu
software school
Yunnan University
Yunnan, China
x07191822@163.com

Zhiling Zhu
software school
Yunnan University
Yunnan, China
leoniddankt@mail.com

Xingcheng Guo
software school
Yunnan University
Yunnan, China
rxij4vcol3@mail.com

Wei Wang^{*}
software school
Yunnan University
Yunnan, China
wangwei@ynu.edu.cn

Abstract—Over the past fifty years, numerous software defect prediction (SDP) approaches have been proposed. However, the ability to explain why predictors make certain predictions remains limited. Explainable SDP has emerged as a promising solution by using explainable artificial intelligence (XAI) methods to clarify the decision-making processes of predictors. Despite this progress, there is still significant potential to enhance the reliability of existing approaches. To address this limitation, we treat defect prediction and the corresponding interpretation as two distinct but closely related tasks and propose a joint learning framework that allows for the simultaneous training of the predictor and its interpreter. The novelty of our approach lies in two main aspects: 1. We design feedback loops that convey the decision-making logic from the predictor to the interpreter. This ensures a high level of conciseness in decision logic and feature engineering for both the predictor and the interpreter, enabling the interpreter to achieve reliable local and global interpretability. 2. We incorporate the interpretation results as a penalty term in the loss function of the joint-learning framework. This not only improves the accuracy of the predictor but also imposes a stronger constraint on the reliability of the interpreter. We validated our proposed method against several existing explainable SDPs across multiple datasets. The results demonstrate its effectiveness in both interpretation and defect prediction. The source code for the proposed method is available at: <https://github.com/BugPredictor/software-defect-prediction.git>

Index Terms—software defect prediction, interpretability, knowledge distillation, joint learning framework

I. INTRODUCTION

For nearly half a century, software defect prediction (SDP) has been a significant research focus in the field of software engineering [1], [2]. Its primary aim is to identify defective code early in the software development process, helping practitioners prioritize quality assurance tasks, especially when resources are limited or deadlines are tight [49]. Inspired by the success of machine learning (ML) in various disciplines, such as computer vision and machine translation, researchers have explored applying different ML algorithms to improve the

accuracy of SDP. However, despite numerous efforts, existing SDP models often fail to provide actionable guidance for practitioners, making practical application challenging [51].

Recent studies have highlighted that the limited applicability of SDP in real-world scenarios is closely linked to the lack of interpretability [3], [4]. Interpretability refers to the ability to provide comprehensible insights into the decision-making logic for humans. Without it, developers struggle to understand the logic behind SDP predictions, leading to distrust and reluctance to adopt these techniques [3], [5]. Explaining prediction results can be particularly challenging for ML-based predictors, especially those using deep learning (DL). The complex structures and large number of parameters in such models obscure straightforward interpretation.

To address this issue, researchers have investigated the feasibility of explainable SDP, incorporating explainable artificial intelligence (XAI) into SDP. Efforts in explainable SDP are generally categorized into two groups [6]: *global* and *local* interpretations. *Global* approaches focus on explaining the overall behavior of a defect predictor, offering insights into how the model makes decisions across all instances [7]. *Local* approaches provide clear evidence for why a given instance is predicted as buggy or clean. The prediction results provide actionable guidance for practitioners to address key questions, such as why a specific prediction was made and how to mitigate associated risks [57]. As a result, practitioners often prefer to use local interpretation techniques in practice [3]. Nevertheless, local techniques often encounter challenges with reliability under different settings [52].

To illustrate the challenges associated with *local* approaches, we take the interpretation for "AbstractCommand.java" from the Apache ActiveMQ project as an example. The explanations generated by LIME with different samplers (i.e., SMOTE and RUS) are shown in Fig. 1 (a). The explanations generated by applying LIME twice to the same file are shown in Fig. 1 (b). These figures present the rankings of features that contribute

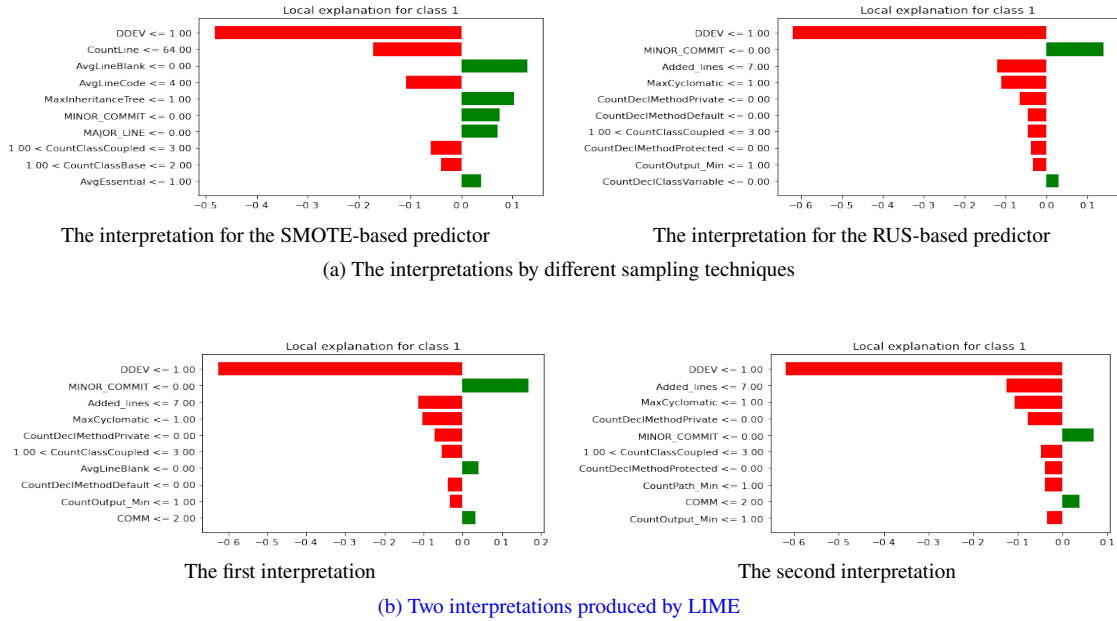


Fig. 1. Interpretations of LIME for a code fragment.

to the predictions. Features displayed in red indicate their contribution to predicting buggy code, while those displayed in green indicate their contribution to the prediction of clean code.

In Fig. 1 (a), we can see that although the SDP model with different samplers predicts the file as buggy, their explanations vary significantly. Among the ten features selected by LIME for the SMOTE-based predictor, only two are also selected for the RUS-based predictor. Fig. 1 (b) further demonstrates that the two explanations generated by running the same predictor twice show considerable variation. For instance, in the first explanation, seven features contribute to the prediction of buggy code, whereas in the second explanation, the number increases to eight.

To address this issue, we consider defect prediction and the corresponding interpretation as two distinct but strongly related tasks and propose a joint-learning framework in this paper. Specifically, we design multiple feedback loops between the interpreter and predictor to simultaneously achieve reliable interpretation and high prediction accuracy. The specific contributions are as follows:

- To improve the reliability of interpretation, we revised the loss function of the knowledge distillation (KD) framework and introduced output fidelity loss and feature fidelity loss. This strategy constructs a knowledge transfer loop between the interpreter and predictor, ensuring a high level of conciseness in decision-making logic and feature engineering power.
- To improve the accuracy of the predictor, we incorporate the interpretation results as a penalty term within the loss function of the joint-learning framework. This enables the predictor to capture more discriminative features guided

by the interpretation results while imposing stronger restrictions on the fidelity of the interpreter to the predictor.

- Extensive experiments are conducted on 20 datasets with an in-depth analysis. The results indicate that the joint-learning framework improves both the reliability of interpretation and the accuracy of the predictor.

The paper is organized as follows: [Section II](#) provides an overview of the existing research on SDP and interpretation methods used in SDP. In [Section III](#), we describe our proposed method in detail, while in [Section IV](#), we provide the details of the experiment. In [Section V](#), we discuss the threats to validity. Finally, in [Section VI](#), we present our conclusion and future works.

II. RELATED WORK

This section provides an overview of SDP and explores existing techniques for explainable SDP.

A. Software defect prediction

The primary goal of SDP is to classify code fragments (e.g., method or class) as either clean or buggy. Constructing a typical SDP model involves three steps. The first step is to transform software metrics, such as cohesion, coupling, complexity, encapsulation, inheritance, and size, into corresponding numerical representations [10]. The second step labels code fragments as buggy or clean based on post-release defects. These defects can be collected from a Bug Tracking System (BTS) by connecting bug reports to their bug-fixing activities. Code fragments associated with these bug-fixing activities are regarded as buggy, while all others are labeled as clean. Finally, the labeled code fragments serve as training data for an ML-based classifier, which is then used to predict whether code fragments in a later version are buggy or clean.

Numerous ML algorithms, including Fuzzy self-organizing maps, K-means, SVM, random forest, logistic regression, etc., have been extensively employed in previous research [15]–[21]. However, metrics used in SDP consistently exhibit correlations and redundancies [11], compromising the effectiveness of traditional ML-based predictors [12]. To address this issue, various DL models have been investigated to improve SDP performance. The initial DL-based defect predictor, Deeper, introduced by Yang et al. [22], employed a deep belief network to identify discriminative information in the input data. Experimental results showed that Deeper could identify 32.22% more defects than many traditional ML-based approaches. Inspired by Yang’s work, many researchers have proposed different DL-based solutions. Specifically, Hoang et al. proposed a convolutional neural network (CNN)-based defect prediction model [23], which experimental results indicated outperformed Deeper. Qiao et al. proposed another DL-based model called DPNN to predict the number of defects [24]. Experimental results showed a 14% reduction in mean square error and an 8% increase in the squared correlation coefficient. Li et al. proposed another CNN-based defect predictor, DP-CNN [25], which achieved better performance than other methods. As demonstrated, DL has significantly improved the performance of SDP.

To ensure the generalization, we employ the DP-CNN proposed in [25] as the predictor and evaluate the difference in accuracy before and after integrating it into the joint-learning framework.

B. Interpretation of defect prediction

In many practical application scenarios, practitioners often ask: What is the underlying decision logic of the predictor? What is the reason for predicting a code fragment as buggy? How do different metrics influence the prediction? These questions highlight an urgent requirement for explainable defect prediction. However, highly accurate SDP models (e.g., Random Forest, DL) are often black-box in nature, making them difficult to interpret.

Efforts to improve the interpretability of predictions can be broadly divided into two main categories [6]: *global* and *local* approaches. The *global* approaches offer a high-level view of how inputs influence the model’s predictions and reveal patterns that are consistent across the model’s entire operation, rather than focusing on individual predictions. Many ML algorithms (e.g., decision trees, logistic regression techniques) and statistical methods (e.g., ANOVA, variable importance) fall into this category [26], [27]. These methods share two common aspects: 1. Simulatability: Every step of the decision-making process is comprehensible. For example, decision trees are simulatable since we can observe the state of every node as well as the feature thresholds used to separate samples. 2. Transparency: The decision-making process can be broken down into interpretable steps. For instance, the interpretability of a decision tree is defined by the computational path from the root node to the leaf nodes. However, *global* approaches cannot provide detailed interpretations for each code fragment, and

their relatively simple structure often fails to guarantee optimal predictive accuracy. Consequently, many practical applications have adopted *local* methods.

In contrast to *global* approaches, *local* methods such as LIME [8] and BreakDown [28], usually interpret the prediction of each code fragment as a list of ordered features. Feedback from practitioners indicates that the interpretations produced by *local* methods can offer more actionable guidance [52]. However, recent studies have reported that *local* techniques lack reliability under various conditions [30], [31], [52]. Firstly, ***the interpretations of the same code can be inconsistent when different data sampling techniques are used.*** In SDP, sampling is frequently used due to the scarcity of buggy codes. It is an effective way to mitigate the effects of imbalanced data on the ML algorithms [53]. In [52], Jiho Shin et al., investigated the consistency of *local* methods across five commonly used data sampling techniques. Their analysis revealed that both the features and the ranking of features in the interpretation vary significantly when different data sampling techniques are employed. Secondly, ***the interpretations of a code fragment do not exhibit consistency when multiple interpretations are executed.*** The underlying intuition of *local* methods regards the interpreter g and the predictor f as two independent ML algorithms and leverages g to approximate the behavior of f within the local area of an instance x , denoted as π_x . In general, *local* methods cannot guarantee that the π_x required for multiple interpretations of the same instance are the same. So different π_x can lead to distinct interpretations for the same code fragment [31]. Finally, ***the predictions produced by the interpreter and the predictor for the same code fragment are not consistent.*** To reduce the difficulty of interpretation, many *local* methods define the interpreter as a simple-structure ML model. Taking the most widely used local interpretation technique LIME as an example, it sets a linear regression model as the interpreter, and the interpretation of SDP is oversimplified as a linear transformation between input metrics and prediction outcomes. Recently, [31] emphasized that attempting to comprehend an intricate model by employing a simple model might be overly optimistic. The inconsistency between the predictions generated by the interpreter and the predictor indicates that the interpretation fails to capture the underlying decision-making logic of the predictor.

C. Knowledge distillation

Knowledge distillation (KD) is a typical model compression technique that transfers knowledge from a teacher model (e.g., DL models) to a student model (e.g., a shallow neural network) [32], [33]. KD is regarded as a promising framework for improving the reliability of interpretation due to the faithful knowledge transfer channel between the student and teacher models. In the health care domain, [34] leveraged distilled knowledge to discover disease patterns. Similarly, in the business domain, [35] distilled dynamical pricing knowledge from a complex black-box DL model, optimizing revenue while maintaining interpretability. In this paper, we designate the

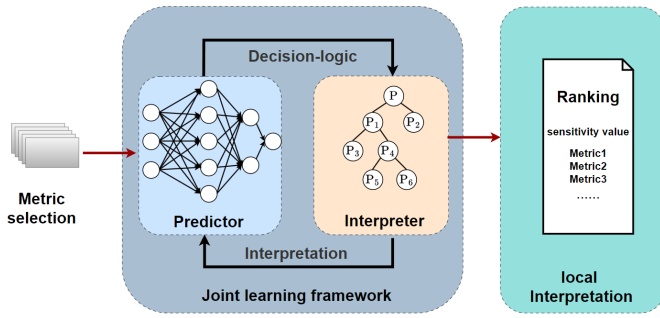


Fig. 2. The framework of our approach.

predictor as the teacher model and the interpreter as the student model, and transfer the decision-making knowledge of predictor to interpreter based on the KD principle. The main difference between our approach and existing methods lies in the revised loss functions of KD framework, which enable us to train the interpreter and predictor in a collaborative manner.

III. PROPOSED METHOD

Fig. 2 provides an overview of our approach, which consists of four modules: metric selection, predictor and interpreter design, joint learning framework, and local interpretation.

A. Metric selection

We carefully selected 16 metrics for our method after a thorough investigation of existing literature and metric suites, including the works of [10], [36], [37]. The details of metrics are presented in Table I. The selection of these metrics was guided by two primary criterias, ensuring their relevance and effectiveness in the context of defect prediction: (1) Expressiveness: The metrics needed to be sufficiently expressive, enabling them to capture subtle variations in code quality, structure, and complexity between similar pieces of source code. (2) Proven Effectiveness: Each selected metric has been validated in prior studies [17], [22], [38], [39], demonstrating its utility in software defect prediction tasks. By adhering to these criterias, we constructed a dataset that covered a broad spectrum of code attributes, ranging from complexity measures to process-related characteristics.

B. Defect prediction and interpretation model

In this section, we provide the detailed information about the predictor and interpreter.

1) *Defect predictor*: To ensure the generality of our method, we chose a DL-based model, DP-CNN [25] as the predictor. It consists of three main components: the convolution layer, max pooling layer, and classification layer. To further improve accuracy, we added an attention layer to the original model. The overall architecture of DP-CNN is presented in Fig. 3.

The working procedure of DP-CNN can be summarized as follows: First, the input defect metrics are fed into the convolution layer to extract correlations between features. Then feature maps are then passed through the max pooling layer, which reduces the dimensionality while retaining the most

TABLE I
METRICS SUITE

Feature	Description
WMC	Weighted methods per class
DIT	Depth of Inheritance Tree
NOC	Number of Children
CBO	Coupling between object classes
RFC	Response for a Class
LCOM	Lack of cohesion in methods
NPM	Number of Public Methods
DAM	Data Access Metric
MOA	Measure of Aggregation
MFA	Measure of Functional Abstraction
CAM	Cohesion Among Methods of Class
IC	Inheritance Coupling
CBM	Coupling Between Methods
AMC	Average Method Complexity
LOC	Lines of Code
CC	McCabe's cyclomatic complexity

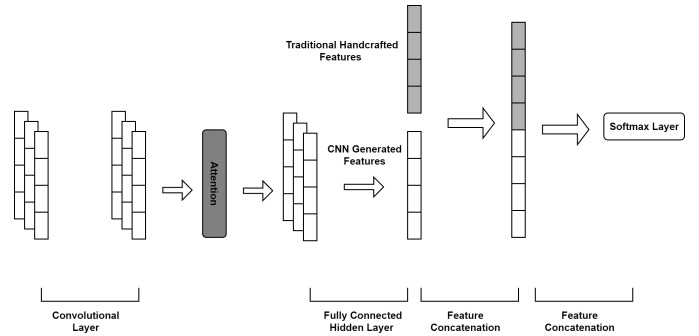


Fig. 3. Model Architecture of DP-CNN.

significant features. To further enhance the model's ability to focus on critical patterns, the attention layer dynamically assigns weights to the feature maps. Finally, the processed features are passed through a fully connected neural network and a softmax classifier to generate the prediction result. The correlations between metrics are crucial for defect prediction. Two characteristics of the convolution layer, sparse connectivity and shared weights, make it particularly suitable for this task [25]. Sparse connectivity enables CNNs to have a wider receptive field, capturing non-linear correlations between metrics. Shared weights ensure that each CNN kernel has the same parameters, allowing predictors to capture these correlations regardless of their position in the input metrics. The max pooling layer retains the most significant features by selecting the maximum local element in the convolutional output, enhancing the model's robustness to changes in the position of metrics in the input. The attention layer dynamically assigns weights to the inputs, providing a flexible way to capture correlations

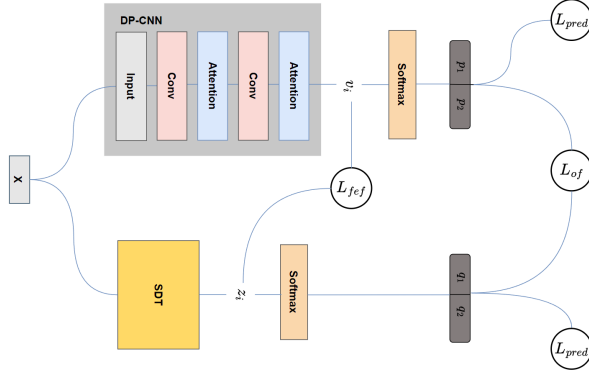


Fig. 4. The architecture of joint learning framework.

between feature maps. The fully connected neural network is responsible for converting the feature maps generated by previous layers into a logit. The softmax block is positioned at the end of the entire neural network, transforming the logits into the probabilities.

2) *Interpretation model*: Following the KD principle, we employ the soft decision tree (SDT) as the interpreter [40]. The SDT is a variant of the fuzzy decision tree, sharing a similar structure with the ordinary decision tree but differing in the definition of nodes. In SDT, nodes are defined as neurons with learnable weight W and bias b . Weights reflect the importance of each feature in the decision-making process at the node. The output of each node is defined as $P_i(x_i) = \sigma(x_i W_i + b_i)$, which determines the probability of transitioning to the right subtree. The $\sigma(\cdot)$ denotes the activation function and x_i is the input of the i -th node. The output at the l -th leaf is defined as:

$$Q_k^l = \frac{\exp(\phi_k^l)}{\sum_k \exp(\phi_k^l)} \quad (1)$$

where Q_k^l is the probability at the l -th leaf of type k defect, and ϕ_k^l is the learned feature at that leaf.

The reasons we use SDT as an interpreter are as follows: Owing to its neural-like node architecture, SDT exhibits comparable feature engineering capabilities to CNN, enabling it to accurately retain the decision-making knowledge of CNN. Furthermore, in comparison to CNN, the complexity of SDT has been reduced, rendering the decision-making process more comprehensible.

C. Joint learning framework

The architecture of the joint learning framework is presented in Fig. 4, each feedback loop corresponds to a specific loss function. **Training stops when the model reaches the maximum number of iterations or meets the early stopping condition.** Given training data set $D = \{(x_i, y_i)_{i=1}^N\}$, $x_i \in R^n$, $y_i \in \{0, 1\}$, the predictor f and interpreter g , the loss function of joint learning framework is formalized as follows:

$$L = \alpha L_{pred}(f, D) + \beta L_{pred}(g, D) + L_{int}(f, g, D) \quad (2)$$

where α and β are hyperparameters.

The original loss function of KD consists of two essential parts: the distillation loss L_{soft} (which is equivalent to $L_{int}(f, g, D)$ in Eq. (2)) and the student loss L_{hard} (which is equivalent to $L_{pred}(g, D)$ in Eq. (2)). L_{soft} quantifies the difference between the teacher model and the student model, which serves as a feedback loop for transferring knowledge from the teacher model to the student model. Minimizing L_{soft} will enforce the student model to adopt similar decision logic to the teacher model. L_{hard} evaluates the difference between the student model's predictions and the ground truth. Minimizing L_{hard} ensures that the student model retains the appropriate decision logic of the teacher model. In this paper, we introduce two key modifications to the existing loss function: (1) added the output fidelity loss $L_{pred}(f, D)$, and (2) revised the L_{soft} .

$L_{pred}(f, D)$ shares a similar definition with $L_{pred}(g, D)$ indicating the consistency of the predictor's output to the ground truth.

$$L_{pred}(f, D) = \sum_{i=1}^{|D|} (f(x_i) - y_i)^2 \quad (3)$$

$$L_{pred}(g, D) = \sum_{i=1}^{|D|} (g(x_i) - y_i)^2 \quad (4)$$

We introduce output fidelity loss guided by two critical considerations: (1) Optimizing the predictor and interpreter simultaneously. Unlike the original KD framework, which keeps the parameters of teacher model (predictor) fixed during the distillation process, minimizing the output fidelity loss will enforce the predictor to capture the discriminative features of the input metrics. (2) Improving the fidelity of the interpreter. Within the KD framework, predictor and interpreter are mutually dependent. Improving the accuracy of the predictor is equivalent to indirectly enforcing the interpreter to provide a more accurate explanation of the predictor's decision logic. Therefore, introducing the output fidelity loss can boost the performance of the predictor and provide a more robust and insightful knowledge based on the KD principle.

Moreover, we revised the loss function L_{soft} (denoted as $L_{int}(f, g, D)$ in Eq. (2)). According to Eq. (5), the $L_{int}(f, g, D)$ involves two parts, $L_{of}(f, g, D)$ and $L_{fef}(f, g, D)$. $L_{of}(f, g, D)$ is equivalent to the distillation loss in the original KD framework. The feature fidelity loss $L_{fef}(f, g, D)$ evaluates the similarity between the feature maps generated by predictor and interpreter. Minimizing $L_{of}(f, g, D)$ and $L_{fef}(f, g, D)$ can enforce the interpreter to adopt similar decision logic and feature engineering power of predictor.

$$L_{int}(f, g, D) = \lambda L_{of}(f, g, D) + \gamma L_{fef}(f, g, D) \quad (5)$$

where λ and γ are hyperparameters. $L_{of}(f, g, D)$ shares a similar definition with $L_{soft}(f, g, D)$, which ensures the

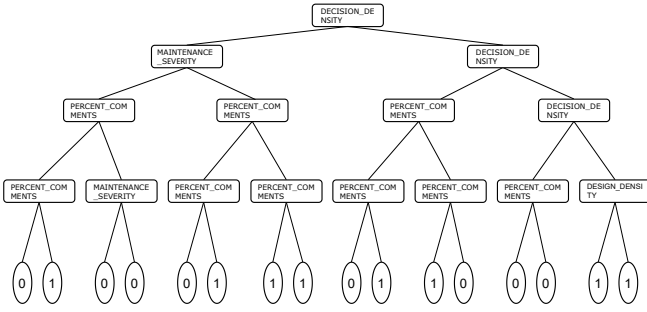


Fig. 5. The interpretations of the proposed method on PC2 dataset.

output of g should be similar to that of f .

$$L_{of}(f, g, T) = - \sum_{i=1}^{|D|} q_i^T \log(p_i^T) \quad (6)$$

where $q_i^T = \frac{\exp(z_i/T)}{\sum_k^N \exp(z_k/T)}$ and $p_i^T = \frac{\exp(v_i/T)}{\sum_k^N \exp(v_k/T)}$ are the classification probability of instance x_i generated by g and f , z_i and v_i are the logits of x_i . T is the temperature hyperparameter [40]. Furthermore, the feature fidelity loss L_{fef} is defined as follows:

$$L_{fef} = \sum_{i=1}^{|D|} (d(z_i) - v_i)^2 \quad (7)$$

where function $d(\cdot)$ adjusts z_i to the same dimension of v_i .

To further clarify the proposed joint learning framework, we take the PC2 dataset as an example. The data in PC2 involves software metrics and labels. Software metrics serve as the input for both the predictor f and interpreter g . Labels indicate whether a code fragment is buggy or clean. The predictor and interpreter were optimized jointly using the loss function defined in Eq. (2). Through the joint training process, the predictor was continuously refined to improve its classification accuracy. This process enables the predictor to effectively distinguish between buggy and clean code fragments. Simultaneously, the interpreter was trained to generate a decision tree that aligns with the predictor’s decision-making logic. Through this process, the predictor was also influenced by the interpreter, as minimizing $L_{int}(f, g, D)$ required the predictor to refine its feature extraction and decision logic to better align with the explanations provided by the interpreter. In Fig. 5, the decision tree generated by the interpreter reflects the optimized decision logic and highlights key decision paths for defect prediction.

D. Local interpretation

It is obvious that SDT obtains the global interpretability as decision tree does [41], and interpretation for a dataset can be abstracted as a set of “IF-THEN” rules. In this section, we focus on the interpretability for an instance. Given a metric set $A = \{a_1, a_2, \dots, a_d\}$, the sensitivity of SDT for an instance x on the a_i is defined as follows.

$$S(a_i) = \frac{\Delta g_i(x)}{\Delta a_i} \quad (8)$$

$\Delta g_i(x) = |g(x) - g(x + \text{One}(a_i)\Delta a_i)|$ is the changes of the output of interpreter aroused by the perturbation of the metric a_i . Δa_i is the standard variance of a_i . $\text{One}(a_i)$ is the onehot encoder of i -the metric.

$$\Delta a_i = \sqrt{\frac{1}{N} \sum_{i=1}^N (a_i - \bar{a})^2} \quad (9)$$

$$\bar{a}_i = \frac{1}{N} \sum_j^N a_j^i \quad (10)$$

where N is the number of training data, and a_j^i is the i -the metric of x_j . According to Eq. (8), we interpret the correlation between the instance and predictive result as the sensitivity of feature perturbation. Given an instance x_i , if a metric has a greater sensitivity, that means such a metric has a stronger influence on the prediction result.

Since the Δa_i is a constant and the parameters of interpreter are fixed after training, the sensitivity S can provide a stable interpretation for any instance. The algorithm for local interpretation is presented below:

Algorithm 1 Local Interpretation

Input: interpreter g , instance x , metric set $A = \{a_1, a_2, \dots, a_d\}$, and hyperparameters: λ, γ .

Output: Sensitivity index SI

- 1: **for** $a_i \in A$ **do**
 - 2: Calculate \bar{a}_i Eq. (10)
 - 3: Calculate Δa_i Eq. (9)
 - 4: Calculate $\Delta g_i(x)$
 - 5: $S = \cup S(a_i)$ Eq. (8)
 - 6: **end for**
 - 7: $SI \leftarrow$ Sorts S in descending order
 - 8: **return** SI
-

The loop structure (lines 2 to 5 in the algorithm) calculates the sensitivity of each metric and generates the sensitivity set S . Line 7 rearranges the sensitivity set S in descending order and puts the index of S to SI .

IV. EXPERIMENT

To objectively evaluate the performance of our method, we conducted an experiment to quantify the performance of the proposed method and the baselines on 20 datasets, aiming to answer the following research questions:

RQ1: What reliability-related improvements does the proposed method make in terms of consistency and faithfulness?

As mentioned in Section II, many *local* methods often yield inconsistent interpretations by adopting different data sampling techniques as well as interpreting the same code fragment multiple times. These two factors greatly affect the reliability of explainable SDP. To evaluate the consistency of interpretation, we adopt the Coincidence Degree (CD) in RQ1

[42]. Given an interpreter g , the CD of an instance x_i is defined as follows :

$$CD(x_i) = \frac{1}{|M|} \left| \bigcap_{j=1}^{|M|} g_j(x_i) \right| \quad (11)$$

where $\bigcap_{j=1}^{|M|} g_j(x_i)$ is the intersection of the multiple interpretations for one instance, $|M|$ represents the number of interpretations or the number of data sampling techniques used. $CD - k\%$ indicates the coincidence of the top k metrics. A greater CD indicates greater consistency.

Furthermore, as discussed in Section II, another issue related to the reliability of interpretation is that predictor and interpreter may generate different predictive results for the same instance. To evaluate the consistency between predictor and interpreter, we introduce Fidelity of Interpretation (FI) [42]–[44] here. Given dataset D , predictor f and interpreter g , the fidelity is defined as:

$$FI = \frac{1}{|D|} \sum_{(x_i, y_i) \in D} \mathbb{I}(f(x_i), g(x_i)) \quad (12)$$

$\mathbb{I}(\cdot)$ is an indicator function, which generates 1 when $f(x_i) = g(x_i)$, 0 otherwise.

In addition to the FI, we argue that the prediction produced by an interpreter should also align with the ground truth. This alignment indicates how much correct decision knowledge is obtained from the predictive model. In this paper, we use the Accuracy of Interpreter (AI) as another indicator to measure this alignment. Given the dataset D and interpreter g , we define the accuracy as:

$$AI = \frac{1}{|D|} \sum_{(x_i, y_i) \in D} \mathbb{I}(g(x_i), y_i) \quad (13)$$

where $|D|$ denotes the cardinality of D , $g(x_i)$ is the prediction made by the interpreter for the instance x_i .

RQ2: What predictive accuracy-related improvements does the proposed method make?

There are two goals in validating the predictor trained by our framework (denoted as Joint_CNN): (1) **The joint learning framework has had a positive impact on the multiple evaluation metrics of the predictor**, and (2) its predictive performance is comparable to other notable predictors. For the first goal, we compare the F-measure and AUC of Joint_CNN with the DP-CNN trained not by our framework (denoted as Base_CNN). In addition, we incorporate three additional metrics from [58]: Percent of Perfect Cleans (PPC), Percent of Non-Perfect Cleans (PNPC), and False Omission Rate (FOR). These indices offer valuable insights into the framework’s ability to balance classification accuracy with practical project management benefits, such as budget savings, remaining time estimates, and failure rate predictions. For the second goal, we compare the F-measure and AUC of Joint_CNN with SVM, Random Forest (RF), and Deep Belief Network (DBN) based predictors. Additionally, although SVM, RF, and DBN are commonly used for classification tasks, they are not

interpretable prediction models. To better demonstrate the effectiveness and advantages of our model, we also included AutoSpearman [13], a widely recognized interpretable prediction model, in the comparison.

The Percent of Pure Cleanings (PPC) measure is defined in [58] as the percentage of correctly predicted negative cases, which indicates the amount of saved budget in the target project. PPC is calculated as:

$$PPC = \frac{|TN|}{|nt|} \quad (14)$$

where TN represents the number of true negatives and $|nt|$ denotes the total number of test instances.

The Percent of Non-Perfect Cleans (PNPC) measure is defined in [58] as the percentage representing the sum of true positives, false positives, and false negatives over the total number of instances tested. This measure is defined as follows:

$$PNPC = \frac{|TP| + |FP| + |FN|}{|nt|} \quad (15)$$

where $|TP|$ represents the number of true positives, $|FP|$ denotes the number of false positives, and $|FN|$ indicates the number of false negatives.

The False Omission Rate (FOR) measure is defined in [58] as the ratio of false negatives over the number of predicted cleans. This is used to estimate the percentage of potential failures that may occur in the target software. FOR is defined as:

$$FOR = \frac{|FN|}{|TN| + |FN|} \quad (16)$$

where $|FN|$ represents the number of false negatives, and $|TN| + |FN|$ is the total number of predicted cleans.

The F-measure, also referred to as the F1-score, assesses the balance between precision and recall. It is the harmonic mean of these two values. The F-measure is defined as:

$$F\text{-measure} = \frac{2 \cdot \text{Precision} \cdot \text{Recall}}{\text{Precision} + \text{Recall}} \quad (17)$$

The Area Under the Curve (AUC) is used to evaluate the performance of binary classification models by measuring the area under its Receiver Operating Characteristic (ROC) curve, which plots the trade-off between true positive rate and false positive rate across different thresholds. The AUC measures the effectiveness of a classification model in distinguishing between defective and non-defective instances. A higher AUC indicates better discrimination, where a value closer to 1 reflects excellent predictive performance.

RQ3: What is the global interpretability of the proposed method?

The objectives of RQ3 are threefold: (1) to demonstrate that our approach obtains global interpretability, (2) to verify its superior computational efficiency, and (3) to demonstrate its reliability. Although local interpretation methods explain the decision logic for a single instance, they fail to reveal the complete structure of predictors [55]. Global interpretable methods can fill in the gaps left by local interpretable methods.

For the first objective, we aim to demonstrate our approach is a decision tree-like interpretable method. The substantial computational expense is a primary disadvantage of current global interpretation methods [56]. For the second objective, we want to quantify the computational efficiency of our method and SP-Lime [55] by comparing the training time of them. The rationale for using SP-Lime as the baseline is as follows. First, SP-Lime is a representative example of perturbation-based global interpretable methods and most global explainable methods are based on the perturbation algorithm [55]. Second, SP-Lime is the global version of Lime (one of baselines of RQ1). Selecting it as baseline is helpful to maintain the consistency of the experiment.

RQ4: What is the effect of different features on the performance and interpretability of our approach?

To assess the impact of individual features on the model’s performance and interpretability, we carried out an ablation experiment. Specifically, we took Joint_CNN as the predictor and eliminated metrics individually. The impacts on the predictor was evaluated by observing changes in the F-measure, AUC, and MCC, and compared these results with the model’s interpretability. MCC is an acronym for Matthews Correlation Coefficient that is used to measure the quality of binary classifications, particularly in imbalanced datasets. The MCC is defined as follows:

$$MCC = \frac{TP \cdot TN - FP \cdot FN}{\sqrt{(TP + FP)(TP + FN)(TN + FP)(TN + FN)}} \quad (18)$$

where TP , TN , FP and FN represent the number of true positives, true negatives, false positives, and false negatives, respectively. The MCC value ranges from -1 to 1, where -1 indicates complete disagreement between predictions and actual outcomes, 1 represents perfect agreement, and 0 implies performance equivalent to random guessing.

A. Dataset

The 20 datasets used in the experiment were collected from the AEEEM ¹, NASA ² and PROMISE ³ repositories. The effectiveness of these datasets has been demonstrated by numerous studies [45]–[48]. Further details about each dataset are provided in Table II. We observe that these datasets exhibit significant class imbalance, with defective instances accounting for only 0.41% of the PC2 dataset.

B. Setting

In the experiment, some parameters were set as follows: the initial learning rate $lr = 1e-06$ and the batch size $batch_size$ is set to 16. The depth of SDT $tree_depth$ is set to 4. The penalty strength of SDT $penalty_strength$ is set to $1e+1$ and the penalty decay rate $penalty_decay$ is set to 0.25. The hyperparameters γ , λ , α and β are set to 0.8, 0.5, 1.4 and 0.6 respectively. The temperature hyperparameter T is set to 100.

TABLE II
DETAILS OF THE DATASETS USED IN THE EXPERIMENT

Group	Dataset	Instances	Defects	%Defects
AEEEM	JDT	997	206	20.66%
	LC	691	64	9.26%
	ML	1862	245	13.16%
	PDE	1492	209	14.01%
NASA	kc1	2109	326	15.46%
	mc1	9466	68	0.72%
	jm1	7782	1672	21.49%
	PC1	549	77	14.03%
	PC2	5589	23	0.41%
	PC3	1563	160	10.24%
	PC4	1458	178	12.21%
PROMISE	ant-1.7	745	166	22.28%
	camel-1.6	965	188	19.48%
	ivy-1.2	352	40	11.36%
	jedit-4.1	312	79	25.32%
	log4j-1.0	135	34	25.19%
	lucene-2.4	340	203	59.71%
	poi-3.0	442	281	63.57%
	synapse1.2	256	86	33.59%
	xerces-1.3	453	69	15.23%

The window size for the Exponential Moving Average (EMA) ema_win_size is set to 1000. We applied the same set of parameters across all datasets to ensure a fair comparison. The dataset was split into 7:2:1 for training, testing, and validation. The experiments are implemented by TensorFlow 2.3.0 with the NVIDIA GeForce RTX 3090 GPU.

1) *Baseline:* We utilize LIME [8] and BreakDown [28] as baselines for RQ1 and RQ3. We selected these techniques due to the following reasons: (1) These two methods are extensively employed by the SDP research community; (2) LIME, BreakDown, and our approach belong to feature-based interpretation techniques that strive to quantify the correlations between input features and predictive outputs; (3) The theoretical foundations of LIME and BreakDown differ substantially, thereby enriching the diversity of comparisons. LIME approximates the behavior of predictors in a local context, whereas BreakDown calculates the cumulative contribution of each feature to the prediction result.

2) *Data preprocessing:* We leverage normalization and different data sampling techniques to process the imbalanced data. Specifically, normalization is defined as follows:

$$\tilde{x} = \frac{x - \min(D)}{\max(D) - \min(D)} \quad (19)$$

where x is the sample of a dataset, and $\min(\cdot)$, $\max(\cdot)$ are the minimum and maximum operations applied column-wise across the dataset. The features in the dataset exhibit significant differences in value range. Without normalization, features with larger numerical ranges might unfairly influence the model. Normalization ensures that all features are on the same scale, so the model treats them equally in terms of their impact. Moreover, normalization helps the algorithm converge faster and more smoothly. As shown in the Table III, normalizing the data significantly improves the model’s performance compared

¹<https://zenodo.org/record/3362613#.YmuGoNpByUk>

²<http://promise.site.uottawa.ca/SERepository/datasets-page.html>

³<http://promise.site.uottawa.ca/SERepository>

TABLE III
AVERAGE PERFORMANCE OF THE MODELS WITH AND WITHOUT DATA
PREPROCESSING ACROSS ALL DATASETS

	F-measure	AUC
Raw Data	0.5822	0.6041
Preprocessed Data	0.6704	0.7109

to using the raw features. We adopt two sampling techniques to the dataset: SMOTE (Synthetic Minority Oversampling Technique) and RUS (Random Undersampling). The technical details of SMOTE and RUS can be found in [49] and [54]. These techniques address class imbalance in defect prediction tasks but may also affect model interpretability. SMOTE balances the dataset by generating synthetic samples, which may subtly alter the distribution of dataset and distort the contribution of feature to the prediction results. In contrast, RUS reduces the dataset size by randomly removing majority-class samples, potentially simplifying the decision process but at the risk of discarding important information, which may affect the stability of the generated explanations.

3) *Statistical significance test*: To verify the significance of the improvements achieved by our approach, we introduced *Cohen's d* in this section. *Cohen's d* is used to measure the difference between two groups, which can take any value between 0 and infinity. When *Cohen's d* takes values in the ranges $[0, 0.2)$, $[0.2, 0.8)$, and $[0.8, +\infty)$, it indicates that the differences between the two groups are small, medium, and large ⁴. The definition of *Cohen's d* is as follows:

$$Cohen's\ d = \frac{M_1 - M_2}{\sqrt{(SD_1^2 + SD_2^2)/2}} \quad (20)$$

where M_1 and M_2 represent the means of the two group data, and SD_1 and SD_2 represent their standard deviations.

C. Experimental results

The experimental results are presented as follows.

1) *The results of RQ1*: To evaluate the consistency of the interpreter trained by our framework (denoted as Joint_SDT), LIME and BreakDown, we employed each of them to interpret an instance ten times, and calculate the average *CD* for each method. As shown in Table V, the average *CD*-10% of LIME, BreakDown and Joint_SDT are 65%, 74.5%, and 100%. This result suggests that LIME exhibits poor consistency. To further investigate the consistency of LIME, we visualized its outputs in Fig. 6 and calculated the coefficient of variation (CV) for the weights assigned to different metrics across the ten interpretations. The results show that the CV is 42.18%. The high CV suggests that LIME is unable to consistently assign similar weights to the same metric across multiple explanations. We believe this inconsistency is partly due to the sampling technique and the hyperparameters used by LIME.

Furthermore, we conducted a comparison between the interpretations generated by LIME and Joint_SDT in terms of

TABLE IV
THE AI AND FI OF JOINT_SDT AND LIME

	AI		FI	
	LIME	Joint_SDT	LIME	Joint_SDT
JDT	0.8200	0.8200	0.8100	0.9300
LC	0.8143	0.8429	0.8000	0.8714
ML	0.6684	0.9037	0.6791	0.9786
PDE	0.7200	0.7533	0.6533	0.7867
jm1	0.6239	0.8010	0.8793	0.9910
kc1	0.6540	0.8531	0.5355	0.9431
mc1	0.8754	0.9916	0.9155	0.9979
PC1	0.8727	0.8727	0.7091	0.9273
PC2	0.9821	0.9982	0.9714	0.9803
PC3	0.7834	0.9172	0.8471	0.9682
PC4	0.8151	0.9178	0.9041	0.9932
ant-1.7	0.6667	0.7467	0.6667	0.9200
camell.6	0.7010	0.5361	0.7010	0.8144
ivy-1.2	0.8056	0.8333	0.8056	0.9167
jedit-4.1	0.5312	0.7500	0.5312	0.5938
log4j-1.0	0.7857	0.6429	0.7857	0.5714
lucene-2.4	0.5000	0.7059	0.5000	0.7059
poi-3.0	0.4222	0.7778	0.4222	0.8222
synapse-1.2	0.5769	0.6538	0.5769	0.5769
xerces-1.3	0.6522	0.7174	0.6522	0.8478
Average	0.7135	0.8018	0.7173	0.8568
Improvement	12.38%↑	-	19.45%↑	-
<i>Cohen's d</i>	0.6792	-	0.9451	-

TABLE V
AVERAGE *CD*s OF LIME, BREAKDOWN AND PROPOSED METHOD

	LIME	BreakDown	Joint_SDT
Average	65%	74.5%	100%
Improvement	53.85%↑	34.23%↑	-

AI and FI. Since BreakDown does not provide an explicit surrogate function like LIME [8], its AI and FI of BreakDown cannot be calculated. As shown in Table IV, across all projects, Joint_SDT achieves an average improvement of 12.38% in AI and 19.45% in FI compared to LIME. The *Cohen's d* results in the table further confirm that Joint_SDT outperforms LIME, with a large effect size in AI and a moderate effect size in FI.

2) *The results of RQ2*: According to Table VI, we observed that Joint_CNN outperforms Base_CNN in terms of both F-measure and AUC. Across all datasets, Joint_CNN achieves an average improvement of 14.67% in F-measure and 4.85% in AUC compared to Base_CNN. Table VII presents the average performance of Base_CNN and Joint_CNN on three groups: PROMISE, NASA, and AEEEM, evaluated using the metrics PPC, PNPC, and FOR. The results in Table VII show that, compared to Base_CNN, Joint_CNN achieves improvements of 10.43% in PPC, 19.67% in PNPC, and 49.86% in FOR. This indicates that Joint_CNN is more accurate in predicting clean modules, more effective in predicting defective instances on average, and better at reducing false negative instances across the target projects. The *Cohen's d* results indicate a large effect size in F-measure and a moderate effect size in

⁴https://en.wikipedia.org/wiki/Effect_size

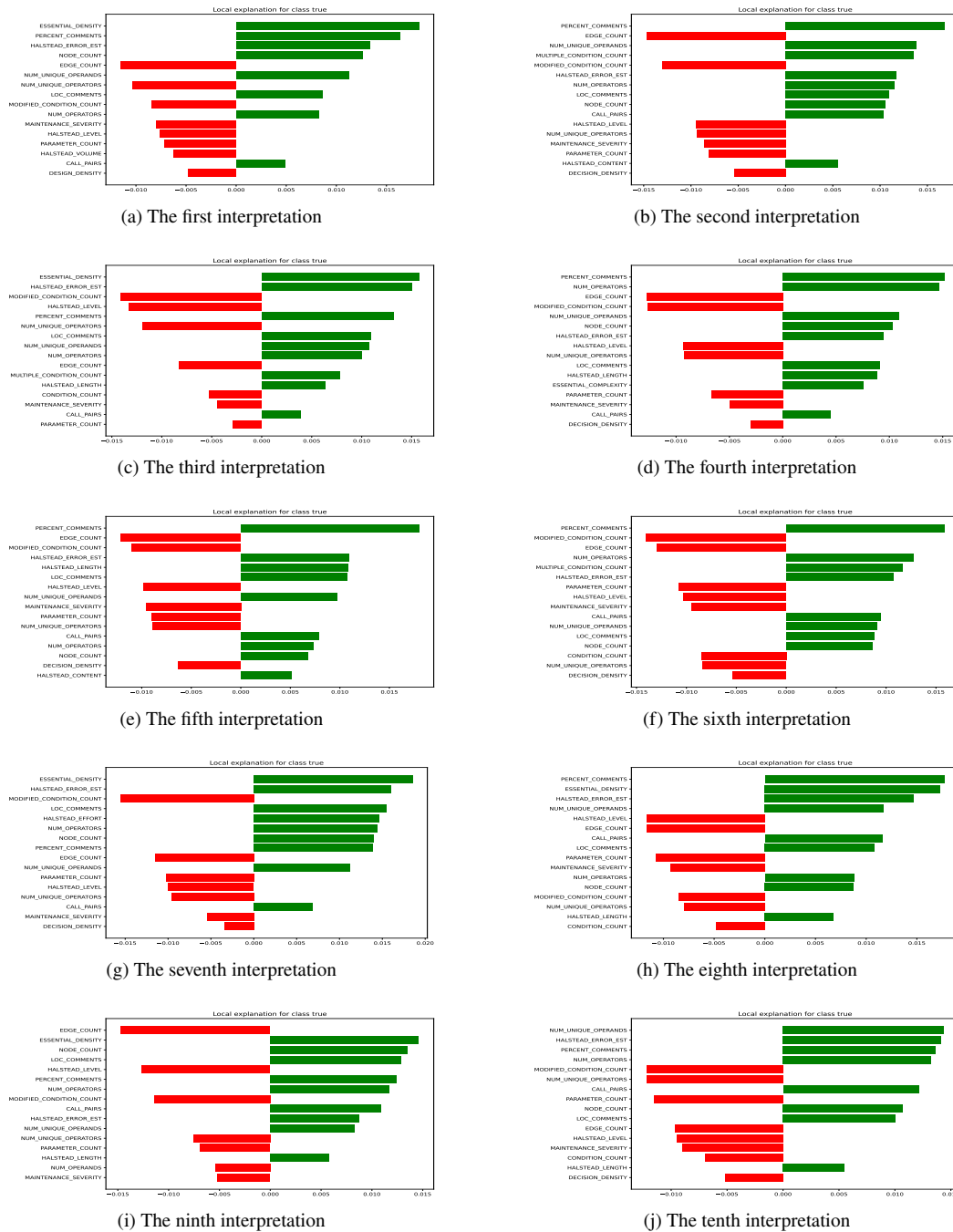


Fig. 6. Multiple interpretations of LIME for a certain instance in the PC2 dataset.

AUC, further confirming the superiority of Joint_CNN over Base_CNN. According to Table VIII, joint_CNN outperforms SVM, RF, DBN and AutoSpearman in terms of both F-measure and AUC. Specifically, Joint_CNN achieves average improvements of 42.86%, 30.63%, 61.75% and 2.13% in F-measure compared to SVM, RF, DBN and AutoSpearman, respectively. Similarly, in AUC, Joint_CNN demonstrates average improvements of 10.93%, 15%, 20.75% and 0.97%. The *Cohen's d* results further validate the performance advantages

of Joint_CNN. In terms of F-measure, the effect sizes are large, indicating significant improvements over SVM, RF and DBN. While the effect size for AutoSpearman is smaller, Joint_CNN still demonstrates overall better performance. For AUC, the effect sizes vary across different comparisons. Specifically, the effect size for SVM is medium, while the effect sizes for RF and DBN are large, indicating significant improvements. Although the effect size for AutoSpearman is small, Joint_CNN still demonstrates overall robustness.

TABLE VI
PREDICTION PERFORMANCE OF JOINT_CNN AND BASE_CNN IN TERMS OF
F-MEASURE AND AUC

	F-measure		AUC	
	Base_CNN	Joint_CNN	Base_CNN	Joint_CNN
JDT	0.6802	0.8544	0.7297	0.8360
LC	0.5686	0.8285	0.6923	0.6862
ML	0.5686	0.7123	0.6897	0.6418
PDE	0.7475	0.7111	0.7039	0.7032
jm1	0.5755	0.8621	0.6240	0.6280
kc1	0.6443	0.7303	0.7545	0.8087
mc1	0.7352	0.8621	0.8082	0.6280
PC1	0.7475	0.8621	0.7039	0.6280
PC2	0.4996	0.8621	0.5000	0.6280
PC3	0.5588	0.7957	0.7634	0.8324
PC4	0.7021	0.7472	0.8169	0.7843
ant-1.7	0.7991	0.7907	0.8276	0.8022
camel-1.6	0.6932	0.7337	0.5992	0.6687
ivy-1.2	0.8273	0.8347	0.6016	0.8594
jedit-4.1	0.5862	0.6946	0.5429	0.8125
log4j-1.0	0.7755	0.6520	0.8500	0.8500
lucene-2.4	0.5623	0.6947	0.5482	0.7643
poi-3.0	0.7156	0.6951	0.7263	0.7414
synapse1.2	0.6616	0.6486	0.8235	0.7516
xerces-1.3	0.7921	0.8407	0.8498	0.7875
Average	0.6720	0.7706	0.7078	0.7421
Improvement	14.67% \uparrow	-	4.85% \uparrow	-
<i>Cohen's d</i>	1.1321	-	0.3553	-

We believe there are two reasons related to the improvement: (1) We explicitly integrate the prediction error $L_{pred}(f, D)$ into the loss function of the joint learning, enabling the predictor to capture discriminative information contained in the data during the training process, and subsequently improving the corresponding accuracy. (2) The L_{int} can be regarded as a penalty term of L , which effectively encourages the framework to learn more generalizable representations of the data, leading to improved predictive accuracy for the data that is not contained in training dataset.

3) *The results of RQ3:* To demonstrate the global interpretability of our approach, we take the PC2 dataset as an example. As presented in Fig. 5, the decision logic can be abstracted as the path from the “DECISION_DENSITY” metric (denoted as the root) to the leaf node (denoted as 1 or 0). For example, one feasible decision path can be presented as DECISION_DENSITY \rightarrow MAINTENANCE_SEVERITY \rightarrow PERCENT_COMMENTS \rightarrow PERCENT_COMMENTS \rightarrow 0, which is similar to the form of decision tree’s interpretation. So, we can conclude our approach achieves the global interpretability.

We measure the computational cost by calculating the average training time. Specifically, we employ the Python time module to record the start and end times of the training process for both our approach and SP-Lime. To ensure statistical reliability, this procedure is repeated ten times for each method. The results show that the average computational costs for our approach and SP-Lime are 744.7 seconds and 2301.4 seconds, respectively. These findings indicate that our method achieves a significant reduction in computational cost compared to

SP-Lime. The substantial difference can be attributed to the optimized design of our method, which abstracts the decision logic as the path of SDT from the root node to the leaf node. In contrast, SP-Lime requires extensive perturbations and evaluations across the feature space, leading to higher computational requirements.

Furthermore, we calculate the CD, FI and AI values for LC dataset to evaluate the reliability of our approach and SP-Lime. As presented in table IX, our method achieves a better performance in all three indicators, indicating our method is more reliable than SP-Lime. The reason for this result can be partially attributed to the random sampling involved in perturbation processes of SP-Lime [55].

4) *The results of RQ4:* We conducted an ablation experiment on 5,589 instances in the PC2 dataset to analyze the impact of different features on model performance. The interpretations generated by our approach are presented in Fig. 5. In the interpretations of our approach, the metrics that have a greater impact on the prediction results are located closer to the root node.

Meanwhile, the impacts on the F-measure, AUC, and MCC after removing certain metrics are presented in Fig. 7. We can see that the accuracy of Joint_CNN went down significantly across MCC, F-measure and AUC three indicators after removing the “DECISION_DENSITY”. This indicates that this metric is critical for the accuracy of the predictor. This finding is consistent with the interpretation of our approach, as our approach placed it at the root node of SDT, indicating its decisive role in the model’s decision-making process. Thus, the significant decline in performance after removing this feature further corroborates its key role in the model. The importance of this feature is strongly evidenced both by the performance change and its position in the explanation.

To enhance the comprehensiveness of the analysis, the ablation experiment was extended to all datasets. The most important features interpreted by our approach for each dataset, as well as the ranking of performance degradation on the F-measure, AUC, and MCC after removing these features, are presented in Table X. The results demonstrate that the performance degradation is consistent with our explanatory results, further validating that our method effectively captures key features to improve prediction performance and provide accurate model interpretations.

V. THREATS TO VALIDITY

While the proposed model demonstrates advancements in both prediction accuracy and interpretability, certain limitations may affect its generalizability and reliability. The details are as follows.

- Choice of dataset: The experiment was conducted on the publicly available datasets. These datasets may not fully capture the diversity of software systems in real-world scenarios, potentially limiting the robustness of the model.
- Hyperparameter setting: The model’s performance is related with the selection of hyperparameters for both the

TABLE VII
AVERAGE PERFORMANCES OF JOINT_CNN AND BASE_CNN IN TERMS OF PPC, PNPC AND FOR

Group	PPC		PNPC		FOR	
	Base_CNN	Joint_CNN	Base_CNN	Joint_CNN	Base_CNN	Joint_CNN
AEEEM	0.6570	0.7394	0.3430	0.2606	0.2597	0.1662
NASA	0.6811	0.7708	0.3189	0.2292	0.0503	0.0256
PROMISE	0.4974	0.5167	0.5026	0.4833	0.1867	0.1398
Average	0.6118	0.6756	0.3882	0.3244	0.1656	0.1105
Improvement	10.43%↑	-	19.67%↓	-	49.86%↓	-

TABLE VIII
THE F-MEASURE AND AUC PERFORMANCE OF DIFFERENT MODELS ON ALL DATASETS

Dataset	F-measure					AUC				
	SVM	RF	DBN	AutoSpearman	Joint_CNN	SVM	RF	DBN	AutoSpearman	Joint_CNN
JDT	0.6239	0.6989	0.7162	0.7824	0.8544	0.7554	0.7419	0.7852	0.8598	0.8360
LC	0.3467	0.7177	0.3467	0.7871	0.8285	0.5846	0.8462	0.5846	0.5046	0.6862
ML	0.4919	0.5958	0.3219	0.8054	0.7123	0.6732	0.7522	0.4596	0.7339	0.6418
PDE	0.5565	0.6209	0.4874	0.7837	0.7111	0.6875	0.6601	0.6130	0.6957	0.7032
jm1	0.4476	0.5849	0.4476	0.7580	0.8621	0.5030	0.5762	0.5030	0.6269	0.6280
kc1	0.5695	0.5371	0.6918	0.5814	0.7303	0.6992	0.6141	0.7724	0.8111	0.8087
mc1	0.4754	0.5513	0.4742	0.5814	0.8621	0.8914	0.5577	0.8326	0.9373	0.6280
PC1	0.3870	0.7556	0.3939	0.8276	0.8621	0.6562	0.8557	0.6057	0.6815	0.6280
PC2	0.4736	0.4996	0.4213	0.9819	0.8621	0.4507	0.5000	0.3647	0.4194	0.6280
PC3	0.5580	0.5745	0.5224	0.8345	0.7957	0.7914	0.5772	0.7356	0.8336	0.8324
PC4	0.5700	0.6694	0.3535	0.8617	0.7472	0.7380	0.6154	0.5651	0.7814	0.7843
ant-1.7	0.7900	0.7121	0.5446	0.7760	0.7907	0.8409	0.7477	0.6591	0.8266	0.8022
camel-1.6	0.4920	0.5367	0.6314	0.6710	0.7337	0.6199	0.5621	0.6923	0.6356	0.6687
ivy-1.2	0.6244	0.7317	0.5000	0.8721	0.8347	0.6719	0.8125	0.7500	0.6250	0.8594
jedit-4.1	0.3914	0.3273	0.3431	0.7585	0.6946	0.4657	0.3743	0.4771	0.8698	0.8125
log4j-1.0	0.4286	0.3538	0.4286	0.6533	0.6520	0.6364	0.5909	0.6364	0.7750	0.8500
lucene-2.4	0.7153	0.3585	0.5983	0.7059	0.6947	0.7140	0.5000	0.6333	0.8250	0.7643
poi-3.0	0.6584	0.6786	0.5139	0.7819	0.6951	0.6463	0.6624	0.5392	0.8082	0.7414
synapse-1.2	0.5439	0.6067	0.3210	0.5247	0.6486	0.5437	0.6062	0.4125	0.6732	0.7516
xerces-1.3	0.6430	0.6865	0.4697	0.7611	0.8407	0.7747	0.6758	0.6465	0.7766	0.7875
Average	0.5394	0.5899	0.4764	0.7545	0.7706	0.6690	0.6453	0.6146	0.7350	0.7421
Improvement	42.86%↑	30.63%↑	61.75%↑	2.13%↑	-	10.93%↑	15.00%↑	20.75%↑	0.97%↑	-
Cohen's d	2.3697	1.7196	2.9703	0.1712	-	0.7337	0.9543	1.1906	0.0657	-

TABLE IX
THE CD, FI AND AI VALUES OF JOINT_SDT AND SP-LIME

Method	CD	FI	AI
Joint_SDT	1.00	0.8714	0.8429
SP-Lime	0.81	0.7933	0.8012

predictor and interpreter. Suboptimal tuning may lead to overfitting or underfitting, resulting in less accurate predictions or interpretations.

- Application scenarios: In this paper, we focus on the within-project defect prediction that the training data and the test data are generated from the same project. However, the performance of our model in the context of the cross-project setting is not evaluated.

VI. CONCLUSION AND FUTURE WORKS

In this paper, we explore the possibility of designing a defect predictor and its corresponding interpreter collaboratively.

Unlike most existing approaches, which treat defect prediction and interpretation as separate tasks, we consider them strongly correlated. Based on this assumption, we introduce a framework aimed at improving the reliability of interpretation while simultaneously enhancing predictive accuracy by utilizing interpretation results. Based on the proposed framework, we conducted extensive empirical evaluations, which revealed the following key findings:

- Compared to existing interpretation methods such as LIME and BreakDown, the proposed framework significantly improves the consistency and reliability of interpretations, providing robust explanations from a local perspective. This improvement is attributed to the incorporation of the Knowledge Distillation (KD) principle, which enables the accurate transfer of decision-making knowledge from the predictor to the interpreter.
- The framework demonstrates superior performance on widely used datasets in terms of both F-measure and AUC, outperforming baseline models such as SVM, RF,

TABLE X
RANKING OF FEATURE IMPORTANCE BASED ON SDT INTERPRETATIONS AND ABLATION RESULTS

Dataset	Top Feature Identified by SDT	F-measure Rank	AUC Rank	MCC Rank
JDT	WCHU_numberOfMethodsInherited	4	9	5
LC	WCHU_cbo	2	1	1
ML	ck_oo_numberOfPublicMethods	5	9	5
PDE	WCHU_fanOut	3	3	5
jm1	HALSTEAD_DIFFICULTY	7	7	1
kc1	v	1	2	2
mc1	LOC_TOTAL	1	1	1
PC1	branchCount	2	1	1
PC2	DECISION_DENSITY	1	4	1
PC3	DESIGN_DENSITY	4	3	3
PC4	LOC_TOTAL	2	2	1
ant-1.7	mfa	1	5	1
camel-1.6	lcom	4	3	4
ivy-1.2	cam	2	7	4
jedit-4.1	lcom3	6	10	4
log4j-1.0	max_cc	4	4	3
lucene-2.4	dam	1	1	1
poi-3.0	wmc	2	3	2
synapse-1.2	cbo	1	1	4
xerces-1.3	max_cc	2	8	2

DBN, and Base_CNN. By explicitly incorporating interpretation results into the loss function, the framework captures more discriminative information, leading to more robust predictive outcomes.

- The proposed method offers global interpretability, providing developers with transparent global insights and decision-making rationales. This capability ensures that the framework not only achieves high accuracy but also delivers comprehensive explanatory support for real-world defect prediction tasks.
- Ablation analysis further demonstrates that the framework effectively identifies key features that have the greatest impact on prediction outcomes, showcasing its ability to provide reliable explanations that align closely with the actual importance of these features.

Future research will investigate several possibilities to further improve the proposed model, including the following:

- Expand the research by including a wider array of datasets that accurately reflect real-world software systems. Evaluate the robustness and generalizability of our model accordingly.
- Incorporate automatic hyperparameter optimization methods into our model to reduce the likelihood of suboptimal tuning.
- Assess the model’s performance in several defect prediction scenarios, such as the cross-project defect prediction.

REFERENCES

- [1] W. Zhang et al., “Research on software defect prediction method based on machine learning,” *Applied Mechanics and Materials*, vol. 687, pp. 2182–2185, 2014.
- [2] Q. Wang, S. Wu, and M. S. Li, “Software defect prediction,” *Journal of Software*, vol. 19, no. 1, 2008.
- [3] J. Jiarpakdee, C. K. Tantithamthavorn, and J. Grundy, “Practitioners’ perceptions of the goals and visual explanations of defect prediction models,” in 2021 IEEE/ACM 18th International Conference on Mining Software Repositories (MSR), pp. 432–443, 2021.
- [4] C. K. Tantithamthavorn and J. Jiarpakdee, “Explainable AI for software engineering,” in 2021 36th IEEE/ACM International Conference on Automated Software Engineering (ASE), pp. 1–2, 2021.
- [5] H. K. Dam, T. Tran, and A. Ghose, “Explainable software analytics,” in *Proceedings of the 40th International Conference on Software Engineering: New Ideas and Emerging Results*, pp. 53–56, 2018.
- [6] W. J. Murdoch, C. Singh, K. Kumbier, R. Abbasi-Asl, and B. Yu, “Definitions, methods, and applications in interpretable machine learning,” *Proceedings of the National Academy of Sciences*, vol. 116, no. 44, pp. 22071–22080, 2019.
- [7] J. Jiarpakdee, C. Tantithamthavorn, and A. E. Hassan, “The impact of correlated metrics on defect models,” *arXiv preprint arXiv:1801.10271*, 2018.
- [8] M. T. Ribeiro, S. Singh, and C. Guestrin, “Why should I trust you? Explaining the predictions of any classifier,” *Proceedings of the 22nd ACM SIGKDD International Conference on Knowledge Discovery and Data Mining*, pp. 1135–1144, 2016.
- [9] S. M. Lundberg and S.-I. Lee, “A unified approach to interpreting model predictions,” *Advances in Neural Information Processing Systems*, vol. 30, 2017.
- [10] J. Bansiya and C. G. Davis, “A hierarchical model for object-oriented design quality assessment,” *IEEE Transactions on Software Engineering*, vol. 28, no. 1, pp. 4–17, 2002.
- [11] J. Jiarpakdee, C. Tantithamthavorn, A. Ihara, and K. Matsumoto, “A study of redundant metrics in defect prediction datasets,” in 2016 IEEE International Symposium on Software Reliability Engineering Workshops (ISSREW), pp. 51–52, 2016.
- [12] J. Jiarpakdee, C. Tantithamthavorn, and A. E. Hassan, “The impact of correlated metrics on defect models,” *arXiv preprint arXiv:1801.10271*, 2018.
- [13] J. Jiarpakdee, C. Tantithamthavorn, and C. Treude, “AutoSpearman: Automatically mitigating correlated software metrics for interpreting defect models,” in 2018 IEEE International Conference on Software Maintenance and Evolution (ICSME), pp. 92–103, 2018, organization=IEEE Computer Society.
- [14] L. Cai, Y. Fan, M. Yan, and X. Xia, “Just-in-time software defect prediction: Literature review,” *Journal of Software*, vol. 30, no. 5, pp. 1288–1307, 2019.
- [15] I.-G. Czibula, G. Czibula, Z. Marian, and V.-S. Ionescu, “A novel approach using fuzzy self-organizing maps for detecting software faults,” *Studies in Informatics and Control*, vol. 25, no. 2, pp. 207–216, 2016.
- [16] D. Kaur, A. Kaur, S. Gulati, and M. Aggarwal, “A clustering algorithm for software fault prediction,” in *Proceedings of the 2010 International Conference on Computer and Communication Technology (ICCT)*, IEEE, pp. 603–607, 2010.

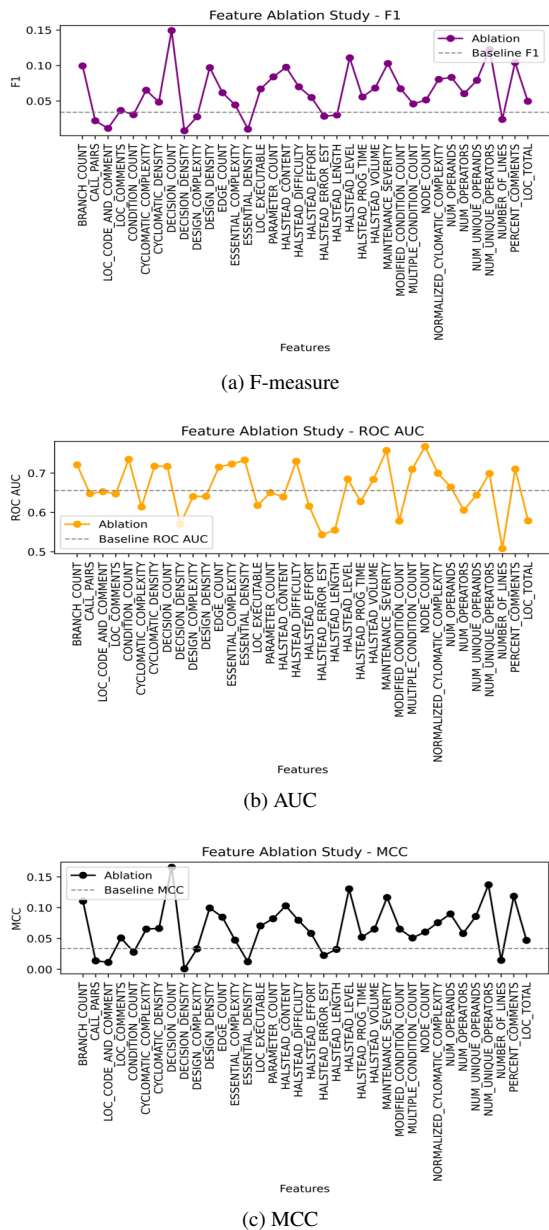


Fig. 7. Ablation study results across multiple indicators. The gray dashed line indicates the performance of DP-CNN before removing metrics.

[17] Y. Kamei et al., “A large-scale empirical study of just-in-time quality assurance,” *IEEE Transactions on Software Engineering*, vol. 39, no. 6, pp. 757–773, 2012, IEEE.

[18] X. Yang, D. Lo, X. Xia, and J. Sun, “TLEL: A two-layer ensemble learning approach for just-in-time defect prediction,” *Information and Software Technology*, vol. 87, pp. 206–220, 2017.

[19] J. Nam, “Survey on software defect prediction,” Department of Computer Science and Engineering, The Hong Kong University of Science and Technology, Tech. Rep, 2014.

[20] B. Eken, “Assessing personalized software defect predictors,” in *Proceedings of the 40th International Conference on Software Engineering: Companion Proceedings*, pp. 488–491, 2018.

[21] T. Jiang, L. Tan, and S. Kim, “Personalized defect prediction,” in *2013 28th IEEE/ACM International Conference on Automated Software Engineering (ASE)*, pp. 279–289, 2013, organization=IEEE.

[22] X. Yang, D. Lo, X. Xia, Y. Zhang, and J. Sun, “Deep learning for just-in-time defect prediction,” in *2015 IEEE International Conference on Software Quality, Reliability and Security*, pp. 17–26, 2015, organization=IEEE.

tion=IEEE.

[23] T. Hoang, H. K. Dam, Y. Kamei, D. Lo, and N. Ubayashi, “Deepjit: An end-to-end deep learning framework for just-in-time defect prediction,” in *2019 IEEE/ACM 16th International Conference on Mining Software Repositories (MSR)*, pp. 34–45, 2019, organization=IEEE.

[24] L. Qiao, X. Li, Q. Umer, and P. Guo, “Deep learning based software defect prediction,” *Neurocomputing*, vol. 385, pp. 100–110, 2020.

[25] J. Li, P. He, J. Zhu, and M. R. Lyu, “Software defect prediction via convolutional neural network,” in *2017 IEEE International Conference on Software Quality, Reliability and Security (QRS)*, pp. 318–328, 2017, organization=IEEE.

[26] M. N. R. Chowdhury, W. Zhang, and T. Akilan, “ANOVA-based Automatic Attribute Selection and a Predictive Model for Heart Disease Prognosis,” *arXiv preprint arXiv:2208.00296*, 2022.

[27] P. Wei, Z. Lu, and J. Song, “Variable importance analysis: A comprehensive review,” *Reliability Engineering & System Safety*, vol. 142, pp. 399–432, 2015.

[28] A. Gosiewska and P. Biecek, “Do not trust additive explanations,” *arXiv preprint arXiv:1903.11420*, 2019.

[29] M. T. Ribeiro, S. Singh, and C. Guestrin, “Anchors: High-precision model-agnostic explanations,” in *Proceedings of the AAAI Conference on Artificial Intelligence*, vol. 32, no. 1, 2018.

[30] J. Yosinski, J. Clune, A. Nguyen, T. Fuchs, and H. Lipson, “Understanding neural networks through deep visualization,” *arXiv preprint arXiv:1506.06579*, 2015.

[31] D. Alvarez-Melis and T. S. Jaakkola, “On the robustness of interpretability methods,” *arXiv preprint arXiv:1806.08049*, 2018.

[32] J. Gou, B. Yu, S. J. Maybank, and D. Tao, “Knowledge distillation: A survey,” *International Journal of Computer Vision*, vol. 129, no. 6, pp. 1789–1819, 2021.

[33] G. Hinton, O. Vinyals, and J. Dean, “Distilling the knowledge in a neural network,” *arXiv preprint arXiv:1503.02531*, 2015.

[34] Z. Che, S. Purushotham, R. Khemani, and Y. Liu, “Interpretable deep models for ICU outcome prediction,” in *Proceedings of the AMIA Annual Symposium Proceedings*, vol. 2016, p. 371, 2016, American Medical Informatics Association.

[35] M. Biggs, W. Sun, and M. Ettl, “Model distillation for revenue optimization: Interpretable personalized pricing,” in *Proceedings of the International Conference on Machine Learning*, pp. 946–956, 2021, PMLR.

[36] M. Jureczko and L. Madeyski, “Towards identifying software project clusters with regard to defect prediction,” in *Proceedings of the 6th International Conference on Predictive Models in Software Engineering*, pp. 1–10, 2010.

[37] M.-H. Tang, M.-H. Kao, and M.-H. Chen, “An empirical study on object-oriented metrics,” in *Proceedings Sixth International Software Metrics Symposium (Cat. No.PR00403)*, pp. 242–249, 1999, organization=IEEE.

[38] L. Qiao and Y. Wang, “Effort-aware and just-in-time defect prediction with neural network,” *PloS One*, vol. 14, no. 2, pp. e0211359, 2019.

[39] K. Zhu, N. Zhang, S. Ying, and D. Zhu, “Within-project and cross-project just-in-time defect prediction based on denoising autoencoder and convolutional neural network,” *IET Software*, vol. 14, no. 3, pp. 185–195, 2020.

[40] N. Frosst and G. Hinton, “Distilling a neural network into a soft decision tree,” *arXiv preprint arXiv:1711.09784*, 2017.

[41] A. Sivaprasad, E. Reiter, N. Tintarev, and N. Oren, “Evaluation of human-interpretability of global model explanations using decision tree,” in *Proceedings of the European Conference on Artificial Intelligence*, Springer, pp. 43–65, 2023.

[42] J. Parekh, P. Mozharovskiy, and F. d’Alché-Buc, “A framework to learn with interpretation,” *Advances in Neural Information Processing Systems*, vol. 34, pp. 24273–24285, 2021.

[43] H. Lakkaraju, N. Arsov, and O. Bastani, “Robust and stable black box explanations,” in *Proceedings of the International Conference on Machine Learning*, pp. 5628–5638, 2020, PMLR.

[44] S. Bang, P. Xie, H. Lee, W. Wu, and E. Xing, “Explaining a black-box by using a deep variational information bottleneck approach,” in *Proceedings of the AAAI Conference on Artificial Intelligence*, vol. 35, no. 13, pp. 11396–11404, 2021.

[45] J. Nam, S. J. Pan, and S. Kim, “Transfer defect learning,” in *2013 35th International Conference on Software Engineering (ICSE)*, pp. 382–391, 2013, organization=IEEE.

[46] R. Wu, H. Zhang, S. Kim, and S.-C. Cheung, “Relink: recovering links between bugs and changes,” in *Proceedings of the 19th ACM*

SIGSOFT Symposium and the 13th European Conference on Foundations of Software Engineering, pp. 15–25, 2011.

- [47] M. D'Ambros, M. Lanza, and R. Robbes, "Evaluating defect prediction approaches: a benchmark and an extensive comparison," *Empirical Software Engineering*, vol. 17, pp. 531–577, 2012.
- [48] F. Peters and T. Menzies, "Privacy and utility for defect prediction: Experiments with morph," in *2012 34th International Conference on Software Engineering (ICSE)*, pp. 189–199, 2012, organization=IEEE.
- [49] N. V. Chawla, K. W. Bowyer, L. O. Hall, and W. P. Kegelmeyer, "SMOTE: synthetic minority over-sampling technique," *Journal of Artificial Intelligence Research*, vol. 16, pp. 321–357, 2002.
- [50] Yan, M., Fang, Y., Lo, D., Xia, X., Zhang, X. . "File-level defect prediction: Unsupervised vs. supervised models," In *2017 ACM/IEEE International Symposium on Empirical Software Engineering and Measurement*, pp. 344-353. 2017.
- [51] Lewis, Chris, Zhongpeng Lin, Caitlin Sadowski, Xiaoyan Zhu, Rong Ou, and E. James Whitehead. "Does bug prediction support human developers? findings from a google case study." In *2013 35th International Conference on Software Engineering (ICSE)*, pp. 372-381. IEEE, 2013.
- [52] Shin J, Aleithan R, Nam J, et al. "Explainable software defect prediction: Are we there yet?". arXiv preprint arXiv:2111.10901, 2021.
- [53] Wang, Song, Taiyue Liu, and Lin Tan. "Automatically Learning Semantic Features for Defect Prediction." In *Proceedings of the 38th International Conference on Software Engineering*. 2016.
- [54] Feng, S., Keung, J., Xiao, Y., Zhang, P., Yu, X., and Cao, X. "Improving the undersampling technique by optimizing the termination condition for software defect prediction," *Expert Systems with Applications*, vol. 235, pp. 121084, 2024.
- [55] Saleem R, Yuan B, Kurugollu F, Anjum A, Liu L. Explaining deep neural networks: A survey on the global interpretation methods. *Neurocomputing*. 2022;513:165-80.
- [56] Bassan S, Amir G, Katz G. Local vs. Global Interpretability: A Computational Complexity Perspective. arXiv preprint arXiv:2406.02981. 2024 Jun 5.
- [57] Yu, J., Fu, M., Ignatiev, A., Tantithamthavorn, C., and Stuckey, P. "A Formal Explainer for Just-In-Time Defect Predictions," *ACM Transactions on Software Engineering and Methodology*, 2024, ACM New York, NY.
- [58] Sharma, U., Sadam, R. "How far does the predictive decision impact the software project? The cost, service time, and failure analysis from a cross-project defect prediction model," *Journal of Systems and Software*, vol. 195, p. 111522, 2023, Elsevier.